Polymers **2015**, *7*, 1674-1688; doi:10.3390/polym7091477

OPEN ACCESS

polymers

ISSN 2073-4360

www.mdpi.com/journal/polymers

Article

Polymeric Shape-Memory Micro-Patterned Surface for Switching Wettability with Temperature

Nuria García-Huete [1], José María Cuevas [2], José Manuel Laza [3], José Luis Vilas [1,3,*] and Luis Manuel León [1,3]

[1] Basque Center for Materials, Applications and Nanostructures (BCMaterials), Parque Tecnológico de Bizkaia, Ed. 500, Derio 48160, Spain; E-Mails: nuria.garcia@bcmaterials.net (N.G.-H.); luismanuel.leon@ehu.eus (L.M.L.)

[2] Gaiker Technology Centre, Parque Tecnológico de Bizkaia, Ed. 202, Zamudio 48170, Spain; E-Mail: cuevas@gaiker.es

[3] Departamento de Química Física, Facultad de Ciencia y Tecnología, Universidad del País Vasco/EHU, Apdo. 644, Bilbao E-48080, Spain; E-Mail: josemanuel.laza@ehu.eus

* Author to whom correspondence should be addressed; E-Mail: joseluis.vilas@ehu.eus; Tel.: +34-94-601-5967; Fax: +34-94-601-3500.

Academic Editor: Wei Min Huang

Received: 7 July 2015 / Accepted: 28 August 2015 / Published: 8 September 2015

Abstract: An innovative method to switch the wettability of a micropatterned polymeric surface by thermally induced shape memory effect is presented. For this purpose, first polycyclooctene (PCO) is crosslinked with dicumyl peroxide (DCP) and its melting temperature, which corresponds with the switching transition temperature (T_{trans}), is measured by Dynamic Mechanical Thermal Analysis (DMTA) in tension mode. Later, the shape memory behavior of the bulk material is analyzed under different experimental conditions employing a cyclic thermomechanical analysis (TMA). Finally, after creating shape memory micropillars by laser ablation of crosslinked thermo-active polycyclooctene (PCO), shape memory response and associated effect on water contact angle is analyzed. Thus, deformed micropillars cause lower contact angle on the surface from reduced roughness, but the original hydrophobicity is restored by thermally induced recovery of the original surface structure.

Keywords: shape memory polymer; laser ablation; wettability; patterning; water contact angle; thermomechanical analysis

1. Introduction

Micro-/nano-topography on surfaces has an outstanding effect on wetting regimes, as it is described by different models dealing with the wettability of patterned surfaces by considering topography [1–4]. For the last years, this approach based on structured surfaces has been used for tailor-made wetting regimes in order to create superhydrophobic, superhydrophilic or superolephobic surfaces, among others [5–7]. Moreover, it is well known that both surface chemistry and surface topography play an important role on the wettability of a material [8], and it can be modified by applying an external stimulus.

Attending to responsive surface chemistry, it can be found light-induced and pH-responsive surfaces. For example, polymers containing acid or basic functional groups (such as amine and carboxyl groups) usually exhibit pH-responsive wetting behavior [9] because their morphologies and/or charges are dramatically influenced by the pH of solution. Among the light-induced surfaces, azobenzene derivatives are very representative, where the wettability varies in presence of light thanks to a *cis–trans* transformation [10,11]. Additionally, these type of materials have been employed to cover a patterned surface in order to obtain superhydrophobic surfaces using light as stimulus [12].

Concerning active surface topography, some examples of patterned surfaces from shape memory polymers by replica molding can be found [13–19] where the recoverability of the patterned structure after being deformed has been demonstrated. Thereby, Xu *et al.* [13] used a semi-crystalline shape memory elastomer to obtain deformable, programmable, and shape-memorizing micro-optical devices. Some authors studied the adhesion properties evaluating it in the different stages of the shape memory process [14–16]. For example, Reddy *et al.* [15] employed a thermoplastic elastomer with thermal shape memory properties to fabricate a switchable adhesive surface. Other authors [17–19] studied if the differences in the wettability of the original and deformed states can be appreciated. For example, Chen and Yang [17] fabricated recoverable tilted pillars from shape memory polymers (an epoxy resin) by replica molding in order to manipulate the surface wettability for potential applications such as directional water shedding and collection.

Shape memory polymers (SMPs) are responsive materials able to recover their original shape under different external stimuli [20,21]. In the particular case of most of the thermo-active shape memory polymers, the shape memory response is based on heating a previously deformed shape above a switching temperature, known as transition temperature (T_{trans}), to recover the original permanent geometry programmed. Thus, the different mobility of macromolecules with temperature acts as the switching mechanism of the macroscale effect [22].

Polycyclooctene (PCO) has previously demonstrated impressive bulk [23–25] and surface [26] shape memory capabilities, where melting temperature of crosslinked network acts as the transition temperature of the thermo-response. Thus, in this work, micropillars based surface structure on crosslinked PCO were designed by laser ablation [27], and interesting variations in water contact angles were observed by means of shape memory features of the PCO micropillars under heating, as seen

in Figure 1. Thus, laser ablation allows fabricating this kind of responsive periodic patterns with high accuracy and reproducibility over large areas, and its combination with handily developed shape memory surface means a broadly applicable and flexible tool to manipulate wettability by heating for platforms where control of fluids is a key facet.

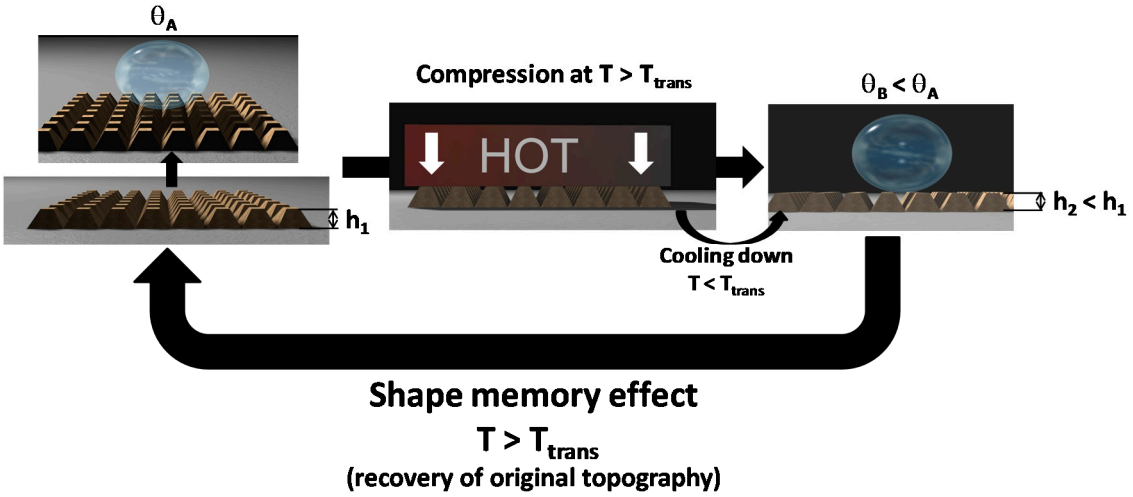

Figure 1. Schematic illustration of switching wettability from thermally induced surface shape memory recovery (from water contact angle θ_A to θ_B by compression, and recovery of the original θ_A by heating).

2. Experimental Section

2.1. Materials

A 99.5% purity low broad molecular weight polyoctenamer from Evonik (Vestenamer® 8012, Marl, Germany) was used as received in pellet form. This polycyclooctene (PCO) consists of linear and cyclic macromolecules with 80% of its double bonds arranged in a crystallizable *trans* configuration. The crosslinking agent was dicumyl peroxide (DCP) from Aldrich (St. Louis, MO, USA), which is a 98.0% purity solid crystalline monofunctional peroxide.

2.2. Preparation of Samples

Polycyclooctene (PCO) and 2 wt % dicumyl peroxide (DCP) were blended as described elsewhere [26] in a Haake Rheomix 600 mixing chamber (Thermo Scientific, Waltham, MA, USA) at 70 °C. Subsequently, the samples were crosslinked at 160 °C for 20 min by compression molding under a pressure of 100 bar in a 1.5 mm thickness flat mold coated with two Teflon sheets to reduce the roughness of the specimens. After curing, the 50 mm × 50 mm × 1.5 mm specimens were cooled down to room temperature in the mold under constant pressure.

The gel content of PCO+2%DCP sample was determined gravimetrically using 10 Soxhlet extraction cycles with boiling cyclohexane as solvent [28]. The obtained gel percentage was about 95%, so this demonstrates the efficiency of crosslinking reaction between PCO and DCP.

Micropillars on crosslinked PCO were manufactured by means of ultrashort pulse laser microprocessing. Femtosecond laser pulses were generated by a Ti:Sapphire oscillator-regenerative

amplifier system (1 kHz, 4.0 mJ, 35 fs pulses at 800 nm, Coherent Inc., Santa Clara, CA, USA). The pulse energy is controlled with a variable neutral density filter in the 1–40 μJ range. The light is focused onto the sample, which is mounted in a computer controlled 3D translation stage (1 μm precision, Thorlabs, Newton, NJ, USA) at atmospheric pressure, using a fused silica lens (f = 150 mm). The diameter of the spot ($FW1/e^2M$) is 40 μm. A nozzle injecting pressurized dry air was placed next to specimens to remove debris. A demonstrative 1 cm^2 surface was structured using 10 μJ/pulse energy and a scanning speed of 0.25 mm/s. In particular, a pattern of lines in two perpendicular directions was generated, with an interval between lines of 46 μm (Figure 2).

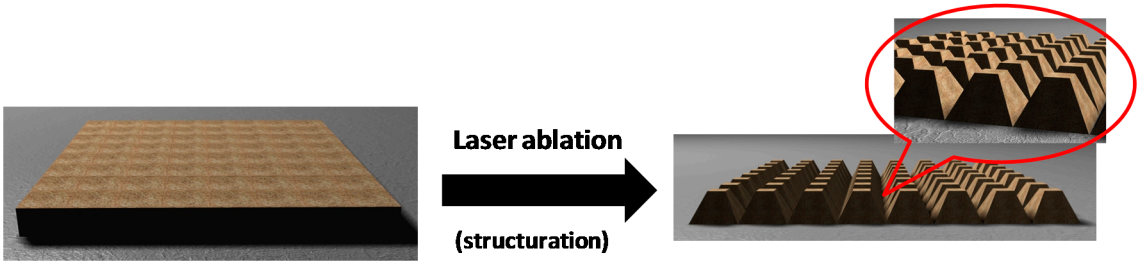

Figure 2. Structuration forming micropillars by laser ablation.

2.3. Experimental Methods

2.3.1. Dynamic Mechanical Thermal Analysis

Dynamic Mechanical Thermal Analysis (DMTA) allows obtaining characteristic temperatures such as glass transition temperature, T_g, and melting temperature, T_m. DMTA was performed in tension mode using a DMA-1 from Mettler Toledo (Greifensee, Switzerland). A rectangular sample (width = 4 mm, thickness = 1.5 mm and free length = 10 mm) was directly cut from the PCO+2%DCP sheet and measured from −100 to 80 °C, at a deformation frequency of 10 Hz, a strain of 100 μm and a heating rate of 2 °C min^{-1}.

2.3.2. Cyclic Thermomechanical Shape Memory Properties

As PCO is a thermally induced shape memory polymer, where the transition temperature corresponds with the melting temperature (T_m), a cyclic thermomechanical experiment was designed in the stress-controlled mode according to Garle *et al.* [29] in order to evaluate the shape memory behavior. Only the crosslinked sample (PCO+2%DCP) was studied by this technique as raw PCO sample flows like a viscous liquid above the melting temperature and does not demonstrate shape memory capabilities.

For thermomechanical analysis (TMA), samples shaped as strips (cut from the PCO+2%DCP sheet) with a cross-section area of 4 × 1.5 mm^2 and initial clamps distance of 10 mm were employed. TMA was also conducted in tension mode on the DMA-1 from Mettler Toledo in the temperature range of −10 to 80 °C at a heating rate of 4 °C min^{-1}. TMA measurements were made following a similar procedure to that reported earlier [30], where the increase of the sample length was recorded as a function of temperature (Figure 3). This temperature range was selected according to the melting temperature previously calculated from calorimetric analysis [26] and corroborated here by DMTA measurements.

The different performed experiments can be appreciate in Table 1, were deformation force or cooling rate were modified in order to study how these parameters affect the fixation of the temporary shape.

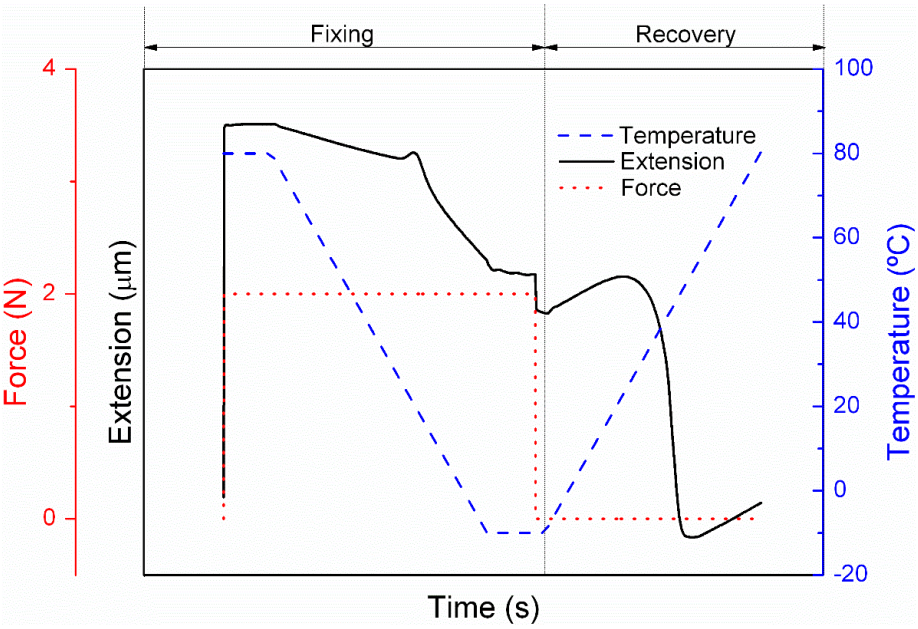

Figure 3. Procedure of the cyclic thermomechanical experiment: extension, temperature and force.

Table 1. Experimental conditions to perform shape memory experiments in bulk material.

Experiment	Force (N)	Cooling rate (°C min^{-1})	Heating rate (°C min^{-1})
1	1	4	4
2	2	4	4
3	2.5	4	4
4	2.5	20	4

2.3.3. Shape Memory Micropillars

Surface micropillars were deformed twice (two cycles) by compression between two neodymium magnets with a pressure of approximately 0.6 MPa on the structured area at a temperature well above T_{trans} (100 °C in the first cycle and 130 °C in the second one), whereas the achieved deformation was fixed immediately by cooling down at room temperature maintaining the pressure. Subsequently, the pressure is removed and the recovery of permanent shape of micropillars was realized by re-heating the sample at 70 °C and letting it cool down.

The height of the micropillars during the respective stages (original, deformed and recovered) in the deformation–fixation–recovery cycles was analyzed by confocal microscopy (Leica LCS SP2 AOBS confocal microscope in reflection mode, Leica Microsystems, Wetzlar, Germany). Furthermore, the analysis of the static water contact angle on achieved structures in each deformation–recovery cycle, as well on the original unstructured PCO surface (Figure 4) as reference, was performed using a video-based optical contact angle measuring system(OCA 15EC from Dataphysics Instruments,

Filderstadt, Germany). All measurements were performed at room temperature with a water drop with approximately 2 μL volume, and resulted from an average of three individual measurements at different positions on the specimen. The different experimental data are summarized in Table 2.

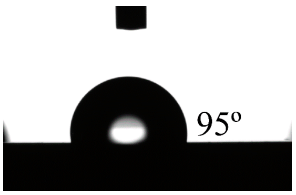

Figure 4. Water contact angle on unstructured crosslinked polycyclooctene (PCO) surface.

Table 2. Height of the micropillars and contact angle on the surface of the PCO+2%DCP sample at the different steps in the shape memory process, Cycle 1 and Cycle 2.

Measured parameters	Initial	Cycle 1		Cycle 2	
		Deformed	Recovered	Deformed *	Recovered
Height (μm)	15.9 ± 0.4	13.1 ± 0.2	15.8 ± 0.4	12.0 ± 0.5	16.2 ± 0.5
Contact angle (°)	136 ± 1.2	124 ± 1.2	135 ± 0.5	120 ± 1.0	136 ± 1.5

* Initial shape in the second cycle corresponds to the recovered shape from the first cycle.

3. Results and Discussion

3.1. Dynamic Mechanical Thermal Analysis

As previously mentioned, DMTA is a widely used technique to obtain characteristic temperatures of polymers, like glass transition temperature, T_g, and melting temperature, T_m. Dynamic mechanical thermal analysis conducted in tension mode was used in this work to confirm the previously reported results obtained by differential scanning calorimetry (DSC) and DMTA in flexion mode for the PCO+2%DCP sample [25,26]. Figure 5 shows both the logarithm of storage modulus (log E') and the loss factor (tanδ = E"/E') measured for that sample.

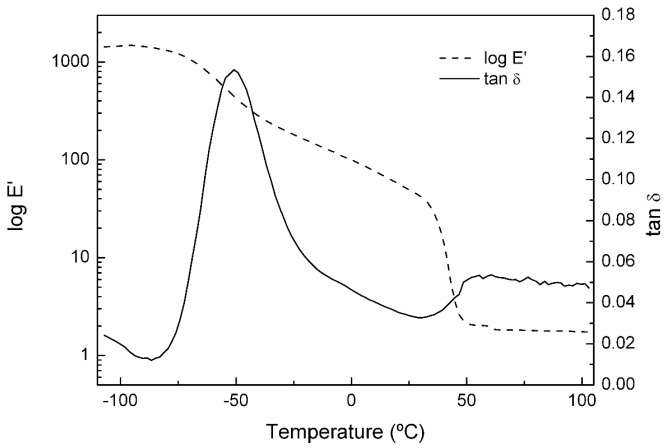

Figure 5. Evolution of tanδ and log E' with temperature for PCO+2%DCP sample.

In Figure 5, it can be observed that initially the polymer is in the glassy state at −100 °C, showing high values of storage modulus and low values of tanδ. As the temperature increases, the storage modulus decreases progressively and a peak appears in tanδ at −50 °C, which corresponds to T_g. Once T_g has been overcome, at temperatures near to the melting transition, the storage modulus decreases sharply, whereas tanδ increases reaching a plateau due to the crosslinks in the PCO+2%DCP preventing the sample to flow like a viscous liquid. As it was expected, this result is in agreement with the previous results from the authors obtained by DMTA in flexion mode [25] and by DSC [26].

3.2. Cyclic Thermomechanical Shape Memory Properties

As already mentioned, shape memory properties of bulk material (PCO+2%DCP sample) were analyzed with a cyclic thermomechanical experiment in tension mode. Shape fixity ratio (R_f) and shape recovery ratio (R_r) for all performed experiments were calculated according to [30] and the obtained values are listed in Table 3. Previously, the sample is heated without force to 80 °C in order to allow relaxation of the polymer chains, so initial conditions are fixed (sample dimensions and temperature). In Figure 6, several thermomechanical cycles for PCO+2%DCP sample are represented. Here, the same cooling rate was used, 4 °C min^{-1}, whereas the deformation force varies from 1 to 2.5 N.

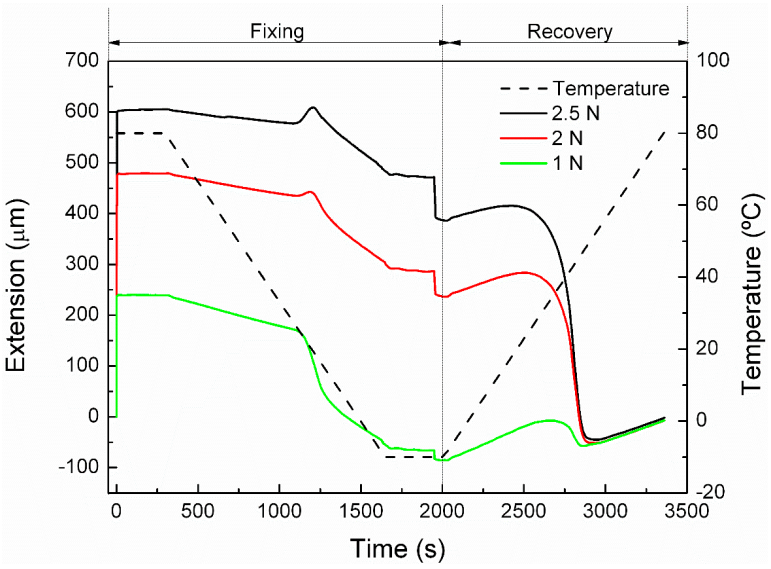

Figure 6. Cyclic thermomechanical response of PCO+2%DCP sample elongated at different forces.

Table 3. Shape fixity and shape recovery ratios for a PCO+2%DCP sample tested at different conditions.

Experiment	R_f (%)	R_r (%)
1	-	100
2	65.0	100
3	65.0	100
4	71.2	100

Thermomechanical cycles demonstrate that higher tensile force involves higher deformation (240 μm for 1 N, 479 μm for 2 N and 604 μm for 2.5 N). The PCO+2%DCP sample was also tested to 3 N but the deformation obtained with this force exceeded the measurement limit of the equipment (1 mm).

After maintaining the stress for 5 min at 80 °C, the sample is cooled down under the same deformation force and shrinkage occurs. It can be observed that too low fixing force (1 N) cannot counteract the contraction stress under cooling ($R_f < 0$), which causes the almost total recovery of original dimensions (0.8% shorter probably from thermal history) before thermal fixing. Therefore, as deformation force increases (2 N and 2.5 N), this one counteracts more efficiently the shrinkage stress and the fixing ratio increases with the applied force.

When the sample is kept at −10 °C for 5 min the deformation stabilizes, stress is removed (leading to springback of the specimen) and temporary shape is fixed (about 1960 s), where higher fixation ratio is observed from increased deformation force. It can be observed that at higher force of deformation, higher is the fixation (R_f with 2 N force = 50.6% and R_f with 2.5 N force = 65.0%, as seen in Table 3).

Finally, the sample is maintained stress-free at −10 °C for 1 min before the recovery process begins by heating the PCO+2%DCP sample to 80 °C, so when temperature reaches T_m, the recovery process takes place and the primary shape is recovered. In all cases, independently of the applied force and thus the generated deformation, the recovery is total.

Therefore, the most remarkable difference between the thermomechanical curves with different tensile forces (1, 2 and 2.5 N) lies in the achieved fixing ratio from higher counteracting shrinkage stress in cooling by higher force (2.5 N). Once the effect of deformation force on the shape memory behavior is analyzed, the next step is to study how the cooling rate affects the fixation process and therefore the shape memory capabilities of the PCO+2%DCP sample.

Therefore, a new thermomechanical cycle is performed by deforming the sample with 2.5 N (maximum deformation and fixing capacity) and cooling at 20 °C min^{-1}. Figure 7 compares the two thermomechanical curves with the two different used cooling rates, 4 and 20 °C min^{-1}, respectively. It can be observed that the two samples elongate equally due to the same deformation force applied. However, when the cooling process takes place faster (20 °C min^{-1}), the sample fixes slightly better the temporary shape, which seems to indicate that the cooling speed has little effect on shape fixity (65.0% *vs.* 71.2%, as seen in Table 3).

Consequently, thermomechanical cycle with a 2.5 N tensile force and 20 °C min^{-1} cooling rate can be considered suitable experimental conditions to study the shape memory behavior of the PCO+2%DCP sample. This thermomechanical cycle was repeated three times (Figure 8), and PCO+2%DCP sample showed a good shape memory behavior, with the ability of coming back to its permanent shape several times (deformation cycles) from potential different temporary shapes.

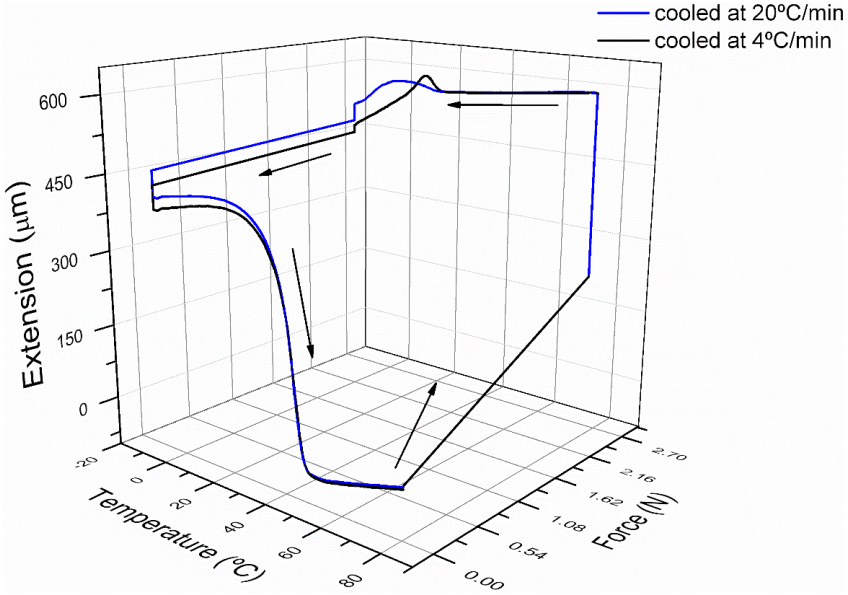

Figure 7. Thermomechanical cycle of PCO+2%DCP sample elongated at 2.5 N force and cooled at different rates.

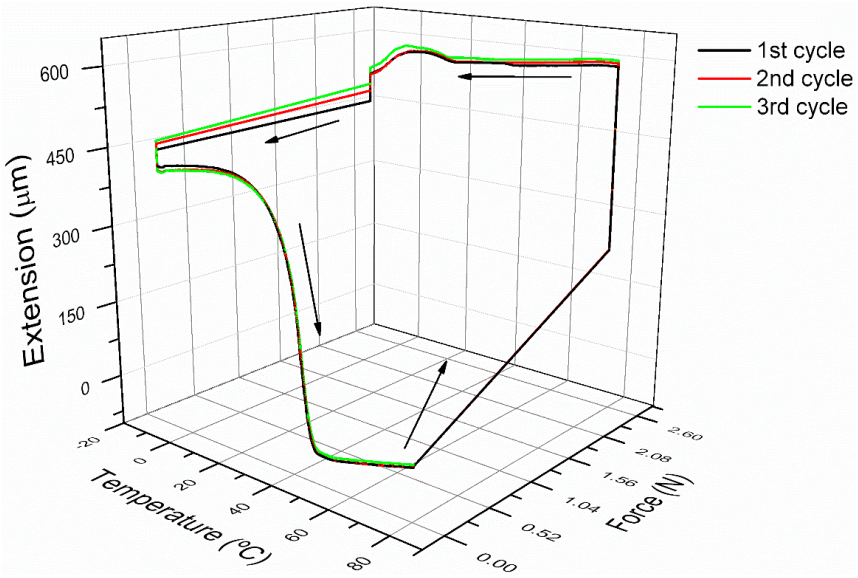

Figure 8. Shape memory capabilities in tension mode of PCO+2%DCP sample.

3.3. Shape Memory Micropillars

Once the PCO+2%DCP sample has been characterized by TMA, micropillars were performed and the shape memory behavior of the microstructure, as well as the wettability, was analyzed.

Starting from a hydrophobic unstructured surface characterized by a water contact angle of $\theta = 95^{\circ}$, the achieved micro-structured surface after femtosecond laser ablation resulted in an outstanding increase of 40° in water contact angle from up to 16 µm height micropillars. As surface analysis (3D representations and XY projections) demonstrated, the obtained micropillars were flat top pyramid-like structures with dissimilar geometry depending on the direction (Figure 9a). Thus, the height in Table 2 was calculated, in all cases, in X direction.

In a first deformation cycle, after the height of the surface micropillars dropped up to 17% as a consequence of the compression stage (Figure 9b), the water contact angle decreased 8.8% approximately, resulting in a less hydrophobic surface than original structured PCO (θ = 124°). Subsequently, this temporally stable less hydrophobic surface, under heating at 70 °C (well above T_{trans}), recovers the original topography taking advantage of the shape memory properties of crosslinked PCO. Consequently, the total recovery of the original height of micropillars, from 100% recovery rate of PCO, restores the higher starting water contact angle (θ = 135°) (Figure 9c).

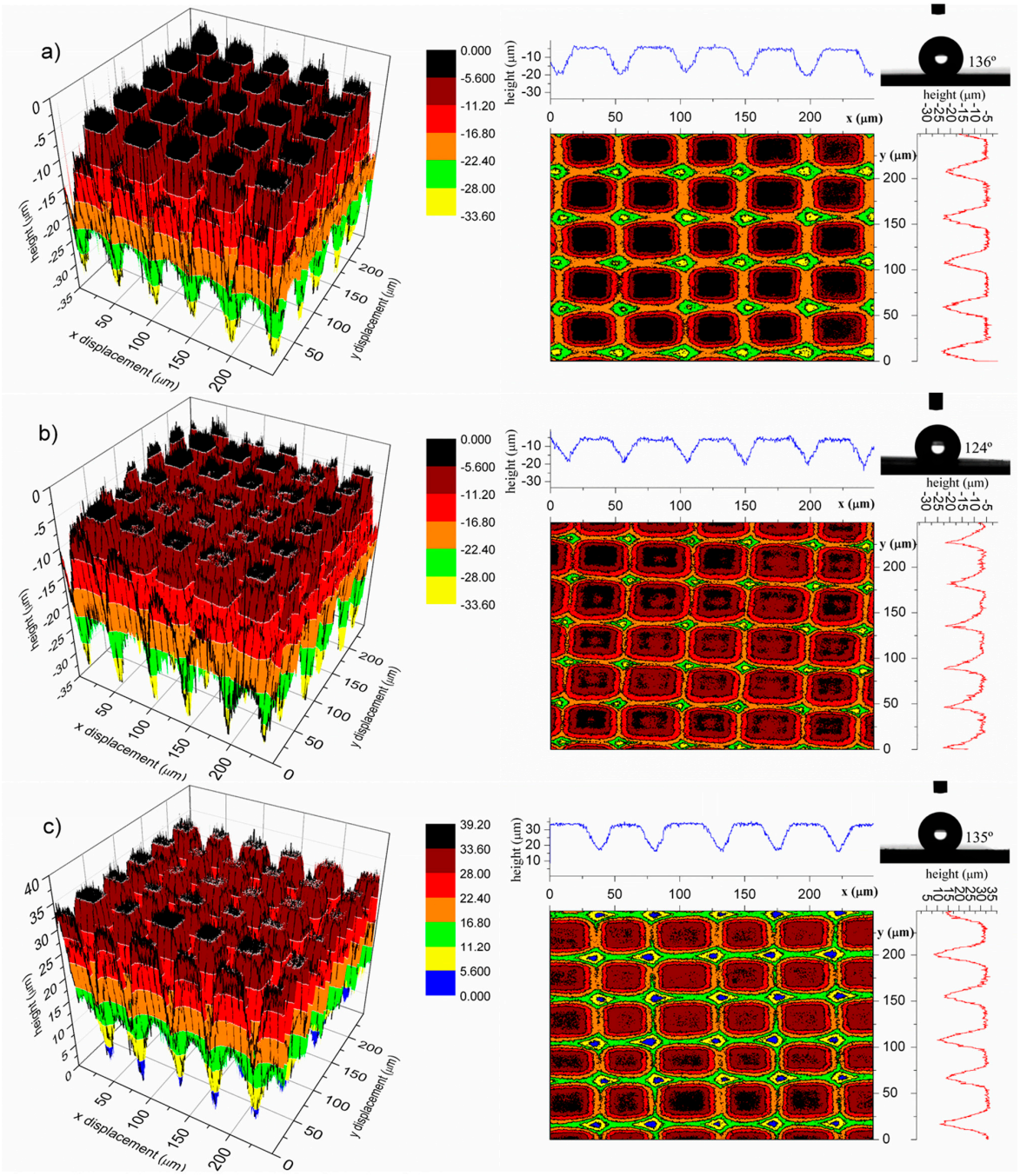

Figure 9. Topography and water contact angle for the first shape memory cycle: (**a**) original; (**b**) deformed (temporal shape); and (**c**) recovered.

In a second deformation–recovery cycle, higher deformation was achieved resulting in micropillars 24% shorter than the original laser ablated surface and, consequently, causing a reduction in the water contact angle up to 11.1%, θ = 120° (Figure 10a). Once again, after heating the sample above the shape memory switching temperature, a 100% recovery of the original topography was observed. Besides, the contact angle returned to the highest value observed from the original structured surface (Figure 10b).

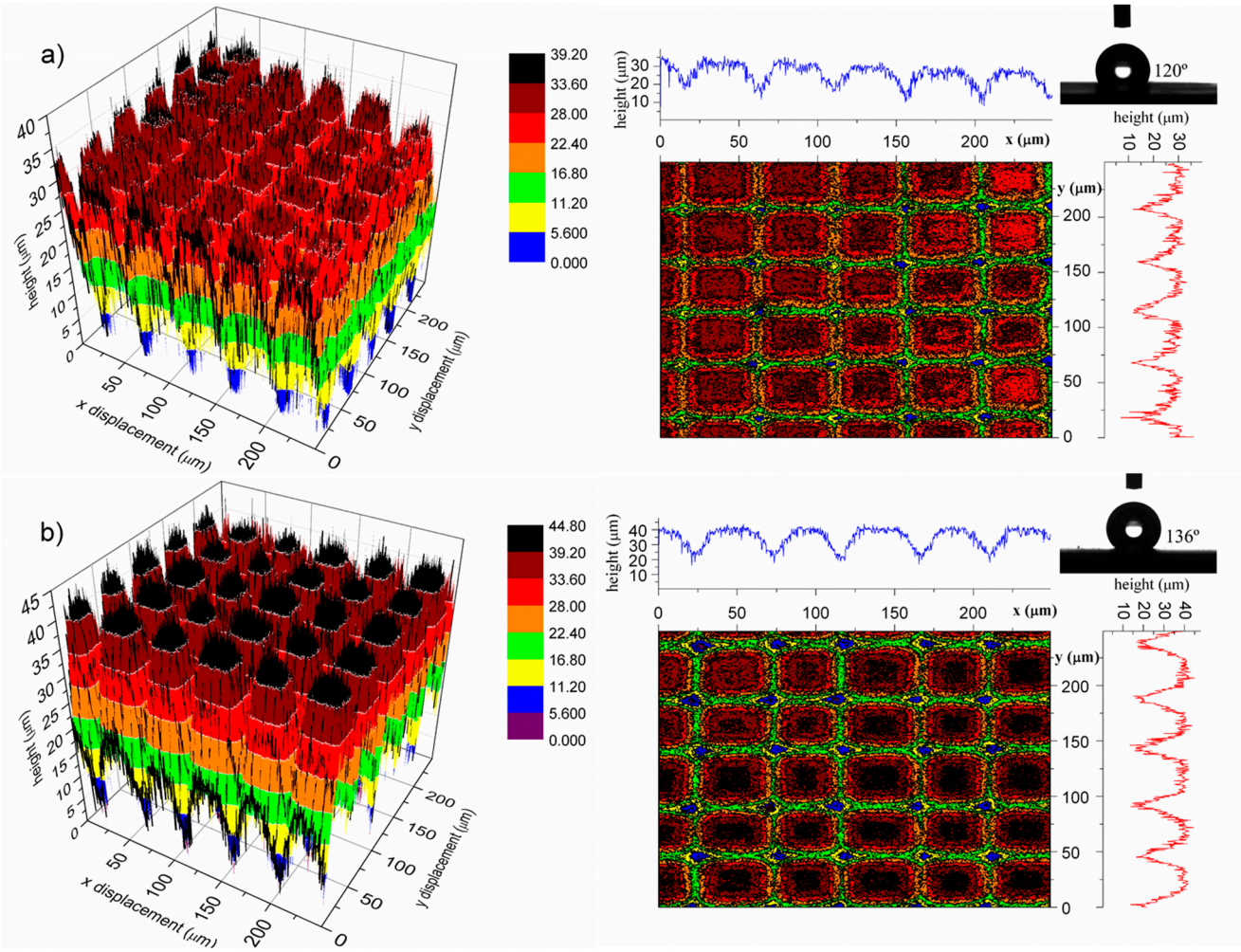

Figure 10. Surface topography and contact angle during the second shape memory cycle: (**a**) deformed (temporal shape) and (**b**) recovered surfaces.

The basic effect of surface roughness can easily be understood by the Wenzel equation [31,32]. The Wenzel's model is usually employed to study the wettability of a rough surface, which is defined by the following equation:

$$\cos\theta_w = r\cos\theta_i \quad (1)$$

In Equation (1), θ_w is the apparent contact angle (corresponds to the stable equilibrium state) and θ_i is the Young's intrinsic contact angle defined for an ideal surface. The roughness ratio, *r*, is a measure of how surface roughness affects a homogeneous surface, defined as the ratio of true area of the solid

surface to the apparent area. Based on this, Shastry *et al.* [33] extracted the equation for a surface of rectangular pillars, shown below:

$$r = \frac{4\,bh + (a+b)^2}{(a+b)^2} \tag{2}$$

In Equation (2), a corresponds to the distance between pillars, b is the pillar width and h is the pillar height. Therefore, from Shastry equation, it can be conclude that the roughness, and then the wettability, depends on the geometry of the pillars and the distance between them.

In this work, the PCO micropillars obtained are not rectangular (the obtained micropillars are flat top pyramid-like structures). Moreover, this equation cannot be applied exactly due to the pillar height varying considerably (up to 24%) when the PCO pillars are deformed, whereas the pillar width and the interpillar distances are, practically, constants (see Figures 9 and 10).

However, this equation can be employed as a simplification to explain the obtained results where a and b can be considered constant. That is, from Shastry equation, the roughness ratio, r, is directly proportional to the pillar height h. Therefore, as in the deformed, state the height decreases, the roughness factor diminishes and the contact angle value is lower. In conclusion, the wettability of a polymeric nanostructured surface can be altered simply by modifying the height of the pillars, as is done in this work through the shape memory behavior.

Considering the three thermomechanical cycles previously made (Figure 8), it could be expected that this deformation–recovery process could repeated an undetermined number of cycles. Furthermore, the variation of wettability with temperature from shape memory recovery of polymer surface topography could be extended to more intermediate scales, unidirectional or reversibly, based on multi-shape memory polymers able to memorize correlated reversible topographies [34,35].

4. Conclusions

The shape memory features of a PCO sample crosslinked with dicumyl peroxide (PCO+2%PDC) have been characterized by TMA in tension mode. On the one hand, the fixing capability of the temporary shape is strongly affected by the deformation force that is mainly responsible for counteracting the thermal shrinkage during cooling at presented low strains. Therefore, higher deformation is retained as applied force increases. However, on the other hand, just a slight effect on fixation is observed with regards to cooling rate.

After performing consecutive TMA cycles (tensile mode) at suitable testing conditions, crosslinked PCO demonstrates outstanding shape memory properties with repeatable behavior as a thermo-responsive polymer.

Once the shape memory response was evaluated, nanostructuring by means of laser ablation has been presented as a suitable method in order to modify the wettability of the polymer surface with high accuracy and reproducibility over large areas (cm^2). As the PCO belongs to the group of thermo-active shape memory polymers with shape memory response based on heating a previously deformed shape above a switching temperature (transition temperature), it is demonstrated that the hydrophobicity (wettability) of this micropatterned polymeric surface can be controlled by means of the thermally induced shape memory effect. Thus, in this work, the wettability measured by water contact angle

changes up to 10% when the shape memory behavior takes place for this monofunctional peroxide based crosslinked commercial polyolefin (PCO+2%DCP).

In particular, the process has been performed twice (two cycles), but it could be expected that this deformation–recovery process could be repeated an undetermined number of cycles taking into account the cyclic TMA results. Definitively, it is possible to control the wettability of the surface by the shape memory effect in a smart way, a fact that could be interesting in different fields such as microfluidics and actuators, among others.

Acknowledgments

The authors thank the Basque Country Government for financial support (Ayudas para apoyar las actividades de los grupos de investigación del sistema universitario vasco, IT718-13). Technical and human support provided by SGIKER (UPV/EHU, MICINN, GV/EJ, ERDF and ESF) is gratefully acknowledged.

Author Contributions

José María Cuevas performed the initial polymer and peroxide mixture. Nuria García-Huete conducted the experimental work and the processing of data and wrote the paper. José María Cuevas, José Manuel Laza, José Luis Vilas and Luis Manuel León contributed to discussion and interpretation of results and contributed to the editing of the paper.

Conflicts of Interest

The authors declare no conflict of interest.

References

1. Marmur, A. Wetting on hydrophobic rough surfaces: To be heterogeneous or not to be? *Langmuir* **2003**, *19*, 8343–8348. [CrossRef]
2. Patankar, N.A. On the modeling of hydrophobic contact angles on rough surfaces. *Langmuir* **2003**, *19*, 1249–1253. [CrossRef]
3. Takeshita, N.; Paradis, L.A.; Öner, D.; McCarthy, T.J.; Chen, W. Simultaneous tailoring of surface topography and chemical structure for controlled wettability. *Langmuir* **2004**, *20*, 8131–8136. [CrossRef] [PubMed]
4. Forward, K.M.; Moster, A.L.; Schwartz, D.K.; Lacks, D.J. Contact angles of submillimeter particles: Connecting wettability to nanoscale surface topography. *Langmuir* **2007**, *23*, 5255–5258. [CrossRef] [PubMed]
5. Jabbarzadeh, A. Effect of nano-patterning on oleophobic properties of a surface. *Soft Matter* **2013**, *9*, 11598–11608. [CrossRef]
6. Jo, H.B.; Choi, J.; Byeon, K.J.; Choi, H.J.; Lee, H. Superhydrophobic and superoleophobic surfaces using ZnO nano-in-micro hierarchical structures. *Microelectron. Eng.* **2014**, *116*, 51–57. [CrossRef]

7. Drelich, J.; Chibowski, E. Superhydrophilic and superwetting surfaces: Definition and mechanisms of control. *Langmuir* **2010**, *26*, 18621–18623. [CrossRef] [PubMed]
8. Zhang, P.; Wang, S.; Wang, S.; Jiang, L. Superwetting surfaces under different media: Effects of surface topography on wettability. *Small* **2015**, *11*, 1939–1946. [CrossRef] [PubMed]
9. Zhang, X.; Shi, F.; Niu, J.; Jiang, Y.; Wang, Z. Superhydrophobic surfaces: From structural control to functional application. *J. Mater. Chem.* **2008**, *18*, 621–633. [CrossRef]
10. Oh, S.-K.; Nakagawa, M.; Ichimura, K. Photocontrol of liquid motion on an azobenzene monolayer. *J. Mater. Chem.* **2002**, *12*, 2262–2269. [CrossRef]
11. Delorme, N.; Bardeau, J.F.; Bulou, A.; Poncin-Epaillard, F. Azobenzene-containing monolayer with photoswitchable wettability. *Langmuir* **2005**, *21*, 12278–12282. [CrossRef] [PubMed]
12. Jiang, W.; Wang, G.; He, Y.; Wang, X.; An, Y.; Song, Y.; Jiang, L. Photo-switched wettability on an electrostatic self-assembly azobenzene monolayer. *Chem. Commun.* **2005**, 3550–3552. [CrossRef] [PubMed]
13. Xu, H.; Yu, C.; Wang, S.; Malyarchuk, V.; Xie, T.; Rogers, J.A. Deformable, programmable, and shape-memorizing micro-optics. *Adv. Funct. Mater.* **2013**, *23*, 3299–3306. [CrossRef]
14. Chen, C.-M.; Chiang, C.-L.; Lai, C.-L.; Xie, T.; Yang, S. Buckling-based strong dry adhesives via interlocking. *Adv. Funct. Mater.* **2013**, *23*, 3813–3823. [CrossRef]
15. Reddy, S.; Arzt, E.; del Campo, A. Bioinspired surfaces with switchable adhesion. *Adv. Mater.* **2007**, *19*, 3833–3837. [CrossRef]
16. Li, W.; Gong, T.; Chen, H.; Wang, L.; Li, J.; Zhou, S. Tuning surface micropattern features using a shape memory functional polymer. *RSC Adv.* **2013**, *3*, 9865–9874. [CrossRef]
17. Chen, C.M.; Yang, S. Directed water shedding on high-aspect-ratio shape memory polymer micropillar arrays. *Adv. Mater.* **2014**, *26*, 1283–1288. [CrossRef] [PubMed]
18. Zheng, Y.; Li, J.; Lee, E.; Yang, S. Light-induced shape recovery of deformed shape memory polymer micropillar arrays with gold nanorods. *RSC Adv.* **2015**, *5*, 30495–30499. [CrossRef]
19. Turner, S.A.; Zhou, J.; Sheiko, S.S.; Ashby, V.S. Switchable micropatterned surface topographies mediated by reversible shape memory. *ACS Appl. Mater. Interfaces* **2014**, *6*, 8017–8021. [CrossRef] [PubMed]
20. Lendlein, A.; Kelch, S. Shape-memory polymers. *Angew. Chem. Int. Ed.* **2002**, *41*, 2034–2057. [CrossRef]
21. Meng, Q.; Hu, J. A review of shape memory polymer composites and blends. *Compos. Part A Appl. Sci. Manuf.* **2009**, *40*, 1661–1672. [CrossRef]
22. Behl, M.; Lendlein, A. Shape-memory polymers. *Mater. Today* **2007**, *10*, 20–28. [CrossRef]
23. Liu, C.; Chun, S.B.; Mather, P.T.; Zheng, L.; Haley, E.H.; Coughlin, E.B. Chemically cross-linked polycyclooctene: Synthesis, characterization, and shape memory behavior. *Macromolecules* **2002**, *35*, 9868–9874. [CrossRef]
24. Cuevas, J.M.; Alonso, J.; German, L.; Iturrondobeitia, M.; Laza, J.M.; Vilas, J.L.; León, L.M. Magneto-active shape memory composites by incorporating ferromagnetic microparticles in a thermo-responsive polyalkenamer. *Smart Mater. Struct.* **2009**, *18*. [CrossRef]

25. Cuevas, J.M.; Laza, J.M.; Rubio, R.; German, L.; Vilas, J.L.; León, L.M. Development and characterization of semi-crystalline polyalkenamer based shape memory polymers. *Smart Mater. Struct.* **2011**, *20*. [CrossRef]
26. García-Huete, N.; Laza, J.M.; Cuevas, J.M.; Gonzalo, B.; Vilas, J.L.; León, L.M. Shape memory effect for recovering surface damages on polymer substrates. *J. Polym. Res.* **2014**, *21*, 481. [CrossRef]
27. Huang, H.; Zheng, H.Y.; Lim, G.C. Femtosecond laser machining characteristics of Nitinol. *Appl. Surf. Sci.* **2004**, *228*, 201–206. [CrossRef]
28. García-Huete, N.; Laza, J.M.; Cuevas, J.M.; Vilas, J.L.; Bilbao, E.; León, L.M. Study of the effect of gamma irradiation on a commercial polycyclooctene I. Thermal and mechanical properties. *Radiat. Phys. Chem.* **2014**, *102*, 108–116. [CrossRef]
29. Garle, A.; Kong, S.; Ojha, U.; Budhlall, B.M. Thermoresponsive semicrystalline poly(ε-caprolactone) networks: Exploiting cross-linking with cinnamoyl moieties to design polymers with tunable shape memory. *ACS Appl. Mater. Interfaces* **2012**, *4*, 645–657. [CrossRef] [PubMed]
30. Axpe, E.; García-Huete, N.; Cuevas, J.M.; Ribeiro, C.; Mérida, D.; Laza, J.M.; García, J.Á.; Vilas, J.L.; Lanceros-Méndez, S.; Plazaola, F.; *et al*. Connecting free volume with shape memory properties in noncytotoxic gamma-irradiated polycyclooctene. *J. Polym. Sci. Part B Polym. Phys.* **2015**, *53*, 1080–1088. [CrossRef]
31. De Gennes, P.-G.; Brochard-Wyart, F.; Quere, D. *Capillarity and Wetting Phenomena: Drops, Bubbles, Pearls, Waves*; Springer: New York, WA, USA, 2004.
32. Wenzel, R.N. Resistance of solid surfaces to wetting by water. *Ind. Eng. Chem.* **1936**, *28*, 988–994. [CrossRef]
33. Shastry, A.; Case, M.J.; Bohringer, K.F. Engineering surface roughness to manipulate droplets in microfluidic systems. *Micro Electro Mech. Syst.* **2005**, 694–697.
34. Cuevas, J.M.; Rubio, R.; German, L.; Laza, J.M.; Vilas, J.L.; Rodriguez, M.; Leon, L.M. Triple-shape memory effect of covalently crosslinked polyalkenamer based semicrystalline polymer blends. *Soft Matter* **2012**, *8*, 4928–4935. [CrossRef]
35. Xie, T. Tunable polymer multi-shape memory effect. *Nature* **2010**, *464*, 267–270. [CrossRef] [PubMed]